ChemComm

Cite this: *Chem. Commun.*, 2011, **47**, 9423–9425

www.rsc.org/chemcomm

COMMUNICATION

In vivo multimode Raman imaging reveals concerted molecular composition and distribution changes during yeast cell cycle†

Chuan-Keng Huang,[a] Hiro-o Hamaguchi[ab] and Shinsuke Shigeto*[a]

Received 22nd April 2011, Accepted 6th July 2011
DOI: 10.1039/c1cc12350e

***In vivo* time-lapse Raman imaging reveals highly dynamic and concerted changes in concentration and distribution of phospholipids and proteins during and after cell division of a single living *Schizosaccharomyces pombe* cell.**

The cell cycle is central to the reproduction of all living organisms. In cell division, the final phase of the cell cycle, vital cellular components including nucleic acids, proteins, membranes and organelles are duplicated accurately and inherited equally by the two daughter cells.[1] This process is exceedingly dynamic in nature in the sense that molecular composition and distribution change continuously before, during and after the cell division. A variety of biochemical and bioanalytical approaches have been developed and employed to elucidate underlying molecular mechanisms of the cell cycle (particularly those of the cell-cycle control[2,3]). However, these methods lack time and space specificity and as a result, the information yielded by those methods is inevitably time- and space-averaged. In fact, quantitative understanding of the dynamic behaviour of molecular composition and distribution in single cells is one of the challenging goals in biological sciences. Here we use Raman microspectroscopy and imaging with a lateral space resolution of 0.3 μm and a time resolution of ~18 min to trace the cell division of a single living *Schizosaccharomyces pombe* cell, *in vivo* and at the molecular level. Multimode Raman images that cover the so-called fingerprint region (800–1800 cm^{-1}) reveal that the concentration and distribution of the two major cellular components, phospholipids and proteins, evolve in a concerted fashion during and after the division of the *S. pombe* cell. Our results demonstrate the potential of the Raman method as a unique tool in single-cell studies including single-cell proteomics[4,5] and metabolomics.[6–8]

Raman spectroscopy, both linear and nonlinear, has been extensively used for studying diverse biological systems *in vivo* under the microscope, because of its noninvasive, nondestructive and label-free characteristics. Living cell systems studied so far include bacteria,[9–11] yeasts,[12–14] blood cells[15,16] and human tissues.[17–19] Among these, a series of meticulous Raman microspectroscopic studies by our group on single budding/fission yeast cells as model organisms have advanced the molecular view of the cellular activities such as cell division[12] and starving cell death.[20] We first observed space-resolved Raman spectra of single living *S. pombe* cells in different cell-cycle phases and kept track of molecular composition changes at the centre of a *S. pombe* cell as it underwent mitosis and cytokinesis.[12] Due to the low sensitivity of the apparatus at the time, we were unable to perform Raman imaging experiments on a dividing cell. We then developed supercontinuum light source-based coherent anti-Stokes Raman scattering (CARS) microscopy,[21] allowing us to acquire CARS images of a dividing *S. pombe* cell.[13] This method achieved higher time resolution (<5 min per image containing two yeast cells[13]) than spontaneous Raman imaging, but only the CARS images of the CH stretching vibrations were obtainable. We have recently developed a high-sensitivity confocal Raman microspectrometer that enables us to carry out Raman imaging measurements for the fingerprint region with sufficiently low laser power (1 mW) and exposure time (1.5 s per pixel in the present case) and to visualize the time course of molecular distributions relevant to the cell-cycle events with high molecular specificity (Fig. S1; see ESI† for details).

Time-lapse Raman images of nine vibrational bands of a dividing *S. pombe* cell over 15 h are presented in Fig. 1, together with the bright-field optical images. The nine Raman images at each time were obtained simultaneously from one two-dimensional scan of the sample. To reduce noise in the Raman spectra recorded with an exposure time of 1.5 s (Fig. S2, ESI†), we employed a numerical post-treatment[11,16,22] based on singular value decomposition (SVD; see ESI†, Fig. S3). Because Raman intensities are proportional to the concentration of the molecule, the image of a Raman band directly visualizes the concentration distribution of the molecular species that gives rise to the Raman band.

First, we discuss the cell-cycle stage at which each Raman imaging measurement is performed on the basis of the cell morphology captured by the optical images (Fig. 1a). When we start the measurement, the target cell chosen randomly is in either the late G_2 phase or the beginning of the M phase (0.5 h, Fig. 1a–1). This is confirmed by the Raman image of a DNA band, which shows the nucleus located around the centre of the cell (Fig. S4, ESI†). By 3 h (Fig. 1a–2), mitosis completes and a

[a] *Department of Applied Chemistry and Institute of Molecular Science, National Chiao Tung University, Hsinchu, Taiwan. E-mail: shigeto@mail.nctu.edu.tw; Fax: +886 3-572-3764; Tel: +886 3-571-2121*
[b] *Department of Chemistry, School of Science, The University of Tokyo, Tokyo, Japan*

† Electronic supplementary information (ESI) available: Details of the experimental methods, comparison of the Raman spectra and images with and without SVD analysis, Raman images of a nucleic acid band, and vibrational mode assignments. See DOI: 10.1039/c1cc12350e

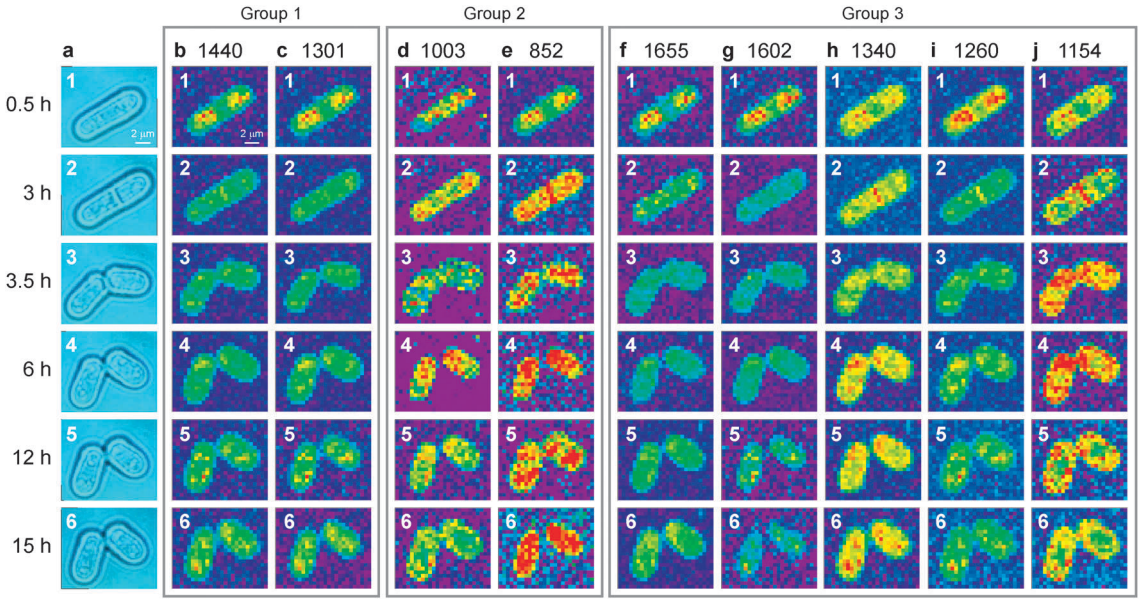

Fig. 1 Time-lapse multimode Raman imaging of a single *S. pombe* cell during its cell cycle. (a) Bright-field optical images of the selected *S. pombe* cell 0.5 (1), 3 (2), 3.5 (3), 6 (4), 12 (5) and 15 (6) h after we started the Raman imaging experiment. Scale bar = 2 μm. (b–j) Images of the Raman bands at 1440 (b), 1301 (c), 1003 (d), 852 (e), 1655 (f), 1602 (g), 1340 (h), 1260 (i) and 1154 (j) cm^{-1} in a rainbow colour scale with red showing the highest intensity and purple the lowest. Full details of the construction of Raman images are given in ESI.† An exposure time of 1.5 s per pixel was used, resulting in a maximum acquisition time of ~18 min for scanning a 11.5 × 16 μm^2 area (23 × 32 pixels). The effective spatial resolution was determined by the step in the scan, *i.e.*, 0.5 μm. The nine Raman images are classified into three groups. Group 1 (b,c), phospholipid Raman images; group 2 (d,e), protein images; and group 3 (f–j), Raman images arising from admixtures of lipids, proteins and other molecular species. Scale bar = 2 μm.

primary septum is formed from plasma membrane to segregate the cell into two compartments, indicating that the cell is in the G_1 or S phase. It is known that *S. pombe* has a very short G_1 phase under normal vegetative conditions, making it difficult to distinguish between the G_1 and S phases in our experiment. At 3.5 h (Fig. 1a–3), cytoplasmic division takes place and the cell splits into two daughter cells. There is no apparent morphological change observed in the G_2 phase (6, 12 and 15 h, Fig. 1a–4–6), where the new cells are thought to grow and duplicate their organelles to prepare for the next division. Note that, although the cell cycle of the selected cell was considerably slowed down compared to the other neighbouring cells, the selected cell showed no noticeable morphological and spectral changes indicative of lethal cellular damage and remained alive throughout and after the experiment.

Next, we discuss the time-lapse Raman images of the dividing *S. pombe* cell (Fig. 1b–j), with the help of the average Raman spectra obtained from the lower end of the cell (Fig. 2a). These Raman images are grouped into three[22] according to mode assignments, intensity distribution patterns and time evolution. Detailed mode assignments[12,23] for both the phospholipid and protein vibrations can be found as Table S1, ESI†. The Raman images of group 1 (Fig. 1b,c) are attributed solely to phospholipids. These images exhibit highly localized distributions. Protein bands constitute the Raman images of group 2 (Fig. 1d,e), showing less heterogeneous distributions that spread over the entire cell(s). Four images in group 3 except for that of 1602 cm^{-1} (Fig. 1f,h–j) consist of the images to which both phospholipid and protein bands possibly contribute (Table S1, ESI†). The band located at 1602 cm^{-1} is an interesting band whose intensity sharply reflects the metabolic activity of yeast cells.[12,24] Although its origin is yet to be clarified, the 1602 cm^{-1} band has been shown to arise exclusively from mitochondria in yeast cells.[12] As manifested by the primary septum seen in Fig. 1h–j–2, polysaccharides seem to also contaminate these three Raman images. The images at 1655 and 1260 cm^{-1} (Fig. 1f,i) display quite similar patterns and time evolution to the lipid images of group 1, strongly indicating that the contribution of phospholipids is dominant in those overlapping Raman bands. In sharp contrast, the images at 1340 and 1154 cm^{-1} (Fig. 1h,j) resemble the protein images of group 2.

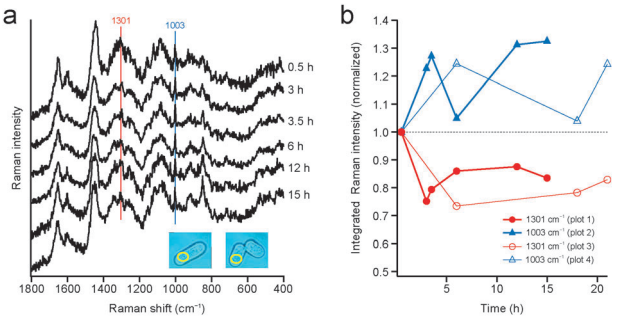

Fig. 2 (a) Time-lapse Raman spectra of the yellow-circled region of the cells (see the optical images in the inset). Each spectrum is an average of 25 spectra that were recorded at different positions inside the circled region. (b) Time dependences of the integrated Raman intensities, *S*, of the bands at 1301 (plot 1) and 1003 (plot 2) cm^{-1}. The Raman intensity of each band (area under the band profile) is summed up over the whole cell(s) (both of the daughter cells for 3.5, 6, 12 and 15 h), then divided by the total number of pixels, *N*, that define the shape of the cell and finally normalized to unity at 0.5 h. That is, $S = \Sigma I_i/N$, where I_i is the Raman intensity at the *i*th pixel in the cell(s). For reference, the time dependences obtained in an independent experiment are also plotted for the two bands (plots 3 and 4).

The method with which we constructed the nine Raman images is based on a univariate analysis. We have adopted this approach because it is simple and intuitive, but it does not allow us to fully extract chemical information from complex Raman spectra of the cell. More detailed analysis using multivariate approaches is now under way and will be reported in a separate publication. Here, in order to avoid uncertainties inherent to the univariate analysis, we shall confine the following discussion to groups 1 and 2, for which the Raman images are unambiguously assigned to phospholipids and proteins, respectively.

How do the molecular composition and distribution within the *S. pombe* cell change as cell division proceeds? At 0.5 h, both phospholipids and proteins appear to be more or less localized near the two ends of the cell. Because the red (high-intensity) patterns in the phospholipid Raman images at this stage (Fig. 1b–1,1c–1) coincide with the mitochondrial distribution reflected by the image of the 1602 cm^{-1} band (Fig. 1g–1), we conclude that the localized pattern can be attributed to high concentrations of phospholipids in mitochondria. The rest of the cell contains phospholipids at lower concentrations than in the mitochondria, as well as other organelles and cytoplasm, resulting in the green (moderate-intensity) pattern. Consistent with the fact that the synthesized biomolecules and organelles are divided equally into the two compartments of the cell, the molecular distribution patterns at 0.5 h are symmetric with respect to the centre of the *S. pombe* cell. At 3 h, when cell division commences, the intensities of the phospholipid bands decrease suddenly from yellow and red to green, whereas those of the protein bands concertedly increase with more even distributions in the cell (compare, for example, Fig. 1b–2 and 1d–2). In the subsequent interphase (3.5–15 h), the intensities of both phospholipids and proteins increase. These findings are fully consistent with the time course of the average Raman spectra (Fig. 2a): the phospholipid-dominant spectrum is seen at the early stages, but after the cell division, the spectrum has more contributions from proteins. To best see this, examine the spectral change in the 1300–1350 cm^{-1} region on going from 0.5 to 15 h. Furthermore, the Raman intensities at 1301 and 1003 cm^{-1} integrated over the whole cell as a function of time (Fig. 2b) provide quantitative information on this concerted behaviour. We have found that the intensity of the phospholipid band (Fig. 2b, plot 1) drops by approximately 20% within the first few hours and rises gradually, synchronously with the continuous increase of that of the protein band by 10–30% (Fig. 2b, plot 2). The other phospholipid and protein bands studied have similar time dependence. The overall trend is reproducible, as demonstrated by plots 3 and 4, which represent the results on another dividing *S. pombe* cell obtained in an independent experiment. The observed concerted behaviour may well indicate that some organelles like mitochondria occur as two different types, namely, phospholipid-rich and protein-rich, depending on the cell-cycle stage.

The highly dynamic and concerted nature of molecular composition and distribution changes in a dividing yeast cell has been revealed for the first time in the present study. It demands that biological investigations now need be done not only at the single-cell level but also with time and space specificity. Recently, mass spectrometry has emerged as a promising label-free method in single-cell analysis.[7,25,26] Despite the ability to identify and quantify molecular species in target cells, mass spectrometry-based methods are destructive, so that it cannot perform time-lapse measurements on one particular cell. In addition, the space resolution of imaging mass spectrometry[26] is still not high enough (typically of the order of 1 μm). Bearing many advantages over mass spectrometry and other biochemical methods, Raman microspectroscopy and imaging should be a valuable, complementary approach for understanding both quantitatively and dynamically the molecular processes that underlie the single-cell activities.

The authors are grateful to National Chiao Tung University for funding the "Ultimate Spectroscopy and Imaging" project. This work was supported in part by Taiwan National Science Council grant 97-2113-M-009-002-MY2 (to S. S.). Prof. Tatsuyuki Yamamoto (Shimane University) is acknowledged for providing the yeast strain.

Notes and references

1 B. Alberts, A. Johnson, J. Lewis, M. Raff, K. Roberts and P. Walter, *Molecular Biology of the Cell*, Garland Science, New York, 2007.
2 P. Nurse, *Trends Genet.*, 1985, **1**, 51–55.
3 L. H. Hartwell and T. A. Weinert, *Science*, 1989, **246**, 629–634.
4 L. Cai, N. Friedman and X. S. Xie, *Nature*, 2006, **440**, 358–362.
5 J. R. S. Newman, S. Ghaemmaghami, J. Ihmels, D. K. Breslow, M. Noble, J. L. DeRisi and J. S. Weissman, *Nature*, 2006, **441**, 840–846.
6 A. Amantonico, J. Y. Oh, J. Sobek, M. Heinemann and R. Zenobi, *Angew. Chem., Int. Ed.*, 2008, **47**, 5382–5385.
7 A. Amantonico, P. L. Urban and R. Zenobi, *Anal. Bioanal. Chem.*, 2010, **398**, 2493–2504.
8 H. Mizuno, N. Tsuyama, S. Date, T. Harada and T. Masujima, *Anal. Sci.*, 2008, **24**, 1525–1527.
9 K. C. Schuster, E. Urlaub and J. R. Gapes, *J. Microbiol. Methods*, 2000, **42**, 29–38.
10 C. Xie and Y.-q. Li, *J. Appl. Phys.*, 2003, **93**, 2982–2986.
11 H. N. Noothalapati Venkata, N. Nomura and S. Shigeto, *J. Raman Spectrosc.*, DOI: 10.1002/jrs.2952.
12 Y.-S. Huang, T. Karashima, M. Yamamoto and H. Hamaguchi, *Biochemistry*, 2005, **44**, 10009–10019.
13 H. Kano and H. Hamaguchi, *Anal. Chem.*, 2007, **79**, 8967–8973.
14 G. P. Singh, G. Volpe, C. M. Creely, H. Grötsch, I. M. Geli and D. Petrov, *J. Raman Spectrosc.*, 2006, **37**, 858–864.
15 G. J. Puppels, J. H. F. Olminkhof, G. M. J. Segers-Nolten, C. Otto, F. F. M. de Mul and J. Greve, *Exp. Cell Res.*, 1991, **195**, 361–367.
16 (*a*) H.-J. van Manen, Y. M. Kraan, D. Roos and C. Otto, *J. Phys. Chem. B*, 2004, **108**, 18762–18771; (*b*) H.-J. van Manen, N. Uzunbajakava, R. van Bruggen, D. Roos and C. Otto, *J. Am. Chem. Soc.*, 2003, **125**, 12112–12113.
17 C. W. Freudiger, W. Min, B. G. Saar, S. Lu, G. R. Holtom, C. He, J. C. Tsai, J. X. Kang and X. S. Xie, *Science*, 2008, **322**, 1857–1861.
18 H.-J. van Manen, A. Lenferink and C. Otto, *Anal. Chem.*, 2008, **80**, 9576–9582.
19 M. Ogawa, Y. Harada, Y. Yamaoka, K. Fujita, H. Yaku and T. Takamatsu, *Biochem. Biophys. Res. Commun.*, 2009, **382**, 370–374.
20 Y. Naito, A. Toh-e and H. Hamaguchi, *J. Raman Spectrosc.*, 2005, **36**, 837–839.
21 H. Kano and H. Hamaguchi, *Opt. Express*, 2005, **13**, 1322–1327.
22 M. Okuno, H. Kano, P. Leproux, V. Couderc, J. P. R. Day, M. Bonn and H. Hamaguchi, *Angew. Chem., Int. Ed.*, 2010, **49**, 6773–6777.
23 P. R. Carey, *Biochemical Applications of Raman and Resonance Raman Spectroscopies*, Academic Press, New York, 1982.
24 (*a*) Y.-S. Huang, T. Nakatsuka and H. Hamaguchi, *Appl. Spectrosc.*, 2007, **61**, 1290–1294; (*b*) C. Onogi and H. Hamaguchi, *J. Phys. Chem. B*, 2009, **113**, 10942–10945.
25 S. S. Rubakhin, E. V. Romanova, P. Nemes and J. V. Sweedler, *Nat. Methods*, 2011, **8**, S20–S29.
26 L. A. McDonnell and R. M. A. Heeren, *Mass Spectrom. Rev.*, 2007, **26**, 606–643.